

FlowAR: Scale-wise Autoregressive Image Generation Meets Flow Matching

Sucheng Ren¹ Qihang Yu² Ju He² Xiaohui Shen² Alan Yuille¹ Liang-Chieh Chen²
¹Johns Hopkins University ²ByteDance

Abstract

Autoregressive (AR) modeling has achieved remarkable success in natural language processing by enabling models to generate text with coherence and contextual understanding through next token prediction. Recently, in image generation, VAR proposes scale-wise autoregressive modeling, which extends the next token prediction to the next scale prediction, preserving the 2D structure of images. However, VAR encounters two primary challenges: (1) its complex and rigid scale design limits generalization in next scale prediction, and (2) the generator’s dependence on a discrete tokenizer with the same complex scale structure restricts modularity and flexibility in updating the tokenizer. To address these limitations, we introduce FlowAR, a general next scale prediction method featuring a streamlined scale design, where each subsequent scale is simply double the previous one. This eliminates the need for VAR’s intricate multi-scale residual tokenizer and enables the use of any off-the-shelf Variational AutoEncoder (VAE). Our simplified design enhances generalization in next scale prediction and facilitates the integration of Flow Matching for high-quality image synthesis. We validate the effectiveness of FlowAR on the challenging ImageNet-256 benchmark, demonstrating superior generation performance compared to previous methods. Codes will be available at <https://github.com/OliverRensu/FlowAR>.

1. Introduction

Autoregressive (AR) models have significantly advanced natural language processing (NLP) by modeling the probability distribution of each token given its preceding tokens, allowing for coherent and contextually relevant text generation. Prominent models like GPT-3 [7] and its successors [29, 30] have demonstrated remarkable language understanding and generation capabilities, setting new standards across diverse NLP applications.

Building on the success of autoregressive modeling in NLP, this paradigm has been adapted to computer vision, particularly for generating high-fidelity images through sequential content prediction [14, 42, 52]. In these ap-

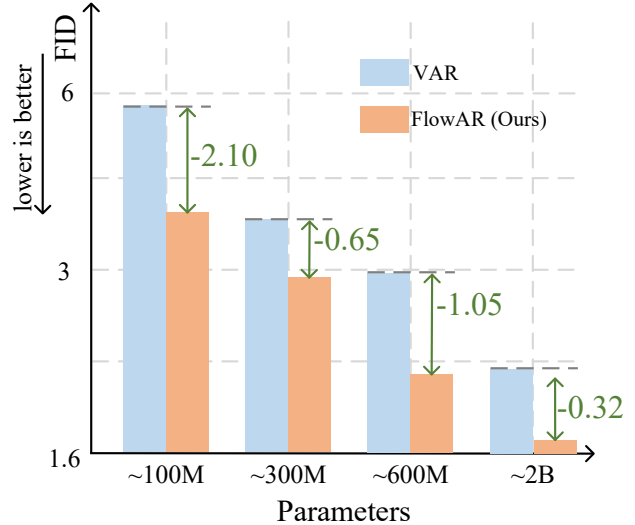


Figure 1. **Performance Comparison.** The proposed FlowAR, a general next-scale prediction model enhanced with flow matching, consistently outperforms state-of-the-art VAR [44] variants across different model sizes.

proaches, images are discretely tokenized, with tokens flattened into 1D sequences, enabling autoregressive models to generate images token-by-token. This approach leverages the sequence modeling strengths of AR architectures to capture intricate visual details. However, directly applying 1D token-wise autoregressive methods to images presents notable challenges. Images are inherently two-dimensional (2D), with spatial dependencies across height and width. Flattening image tokens disrupts this 2D structure, potentially compromising spatial coherence and causing artifacts in generated images. Recently, VAR [44] addresses these issues by introducing scale-wise autoregressive modeling, which progressively generates images from coarse to fine scales, preserving the spatial hierarchies and dependencies essential for visual coherence. This scale-wise approach allows autoregressive models to retain the 2D structure during image generation, capturing the layered complexity of visual content more naturally.

Despite its effectiveness, VAR [44] faces two signif-

icant limitations: (1) a complex and rigid scale design, and (2) a dependency between the generator and a tokenizer that shares this intricate scale structure. Specifically, VAR employs a non-uniform scale sequence, $\{1, 2, 3, 4, 5, 6, 8, 10, 13, 16\}$, where the coarsest scale tokenizes a 256×256 image into a single 1×1 token and the finest scale into 16×16 tokens. This intricate sequence constrains both the tokenizer and generator to operate exclusively at these predefined scales, limiting adaptability to other resolutions or granularities. Consequently, the model struggles to represent or generate features that fall outside this fixed scale sequence. Additionally, the tight coupling between VAR’s generator and tokenizer restricts flexibility in independently updating the tokenizer, as both components must adhere to the same scale structure.

To address these limitations, we introduce FlowAR, a flexible and generalized approach to scale-wise autoregressive modeling for image generation, enhanced with flow matching [25]. Unlike VAR [44], which relies on a complex multi-scale VQGAN *discrete* tokenizer [23, 36], we utilize any off-the-shelf VAE *continuous* tokenizer [22] with a simplified scale design, where each subsequent scale is simply double the previous one (*e.g.*, $\{1, 2, 4, 8, 16\}$), and coarse scale tokens are obtained by directly downsampling the finest scale tokens (*i.e.*, the largest resolution token map). This streamlined design eliminates the need for a specially designed tokenizer and decouples the tokenizer from the generator, allowing greater flexibility to update the tokenizer with any modern VAE [8, 24].

To further enhance image quality, we incorporate the flow matching model [25] to learn the probability distribution at each scale. Specifically, given the class token and tokens from previous scales, we use an autoregressive Transformer [34] to generate *continuous* semantics that condition the flow matching model, progressively transforming noise into the target latent representation for the current scale. Conditioning is achieved through the proposed *spatially adaptive layer normalization* (Spatial-adaLN), which adaptively adjusts layer normalization [3] on a position-by-position basis, capturing fine-grained details and improving the model’s ability to generate high-fidelity images. This process is repeated across scales, capturing the hierarchical dependencies inherent in natural images. The final image is then produced by de-tokenizing the predicted latent representation at the finest scale.

The seamless integration of the scale-wise autoregressive Transformer and scale-wise flow matching model enables FlowAR to capture both the sequential and probabilistic aspects of images with multi-scale information, resulting in improved image synthesis performance. We demonstrate FlowAR’s effectiveness on the challenging ImageNet-256 benchmark [11], where it achieves state-of-the-art results.

2. Related Work

Autoregressive Models. Autoregressive modeling [4, 7, 10, 13, 30, 34, 35, 43, 45, 46, 53] began in natural language processing, where language Transformers [49] are pretrained to predict the next word in a sequence. This concept was first introduced to computer vision by PixelCNN [47], which utilized a CNN-based model to predict raw pixel probabilities. With the advent of Transformers, iGPT [9] extended this approach by modeling raw pixels using Transformer architectures. VQGAN [14, 50] further advanced the field by applying autoregressive learning within the latent space of VQ-VAE [48], thereby simplifying data representation for more efficient modeling [54]. Taking a different direction, Parti [52] framed image generation as a sequence-to-sequence task akin to machine translation, using sequences of image tokens as targets instead of text tokens, and leveraging significant advancements in large language models through data and model scaling. LlamaGen [42] expanded on this by applying the traditional “next token prediction” paradigm of large language models to visual generation, demonstrating that standard autoregressive models like Llama [45] can achieve state-of-the-art image generation performance when appropriately scaled, even without specific inductive biases for visual signals. The work most similar to ours is VAR [44], which transitioned from token-wise to scale-wise autoregressive modeling by developing a coarse-to-fine next scale prediction. However, VAR faces significant challenges due to its complex scale designs and deep dependency on a scale residual discrete tokenizer. In contrast, our proposed FlowAR employs a simple scale design and maintains compatibility with any VAE tokenizer [22].

Flow- and Diffusion-based Models. Diffusion models [18, 19, 24, 26, 31, 37, 41] have surpassed earlier image generation methods like GANs [16, 40] by utilizing multistep diffusion and denoising processes. Latent Diffusion Models (LDMs) [37] advance this approach by transitioning diffusion from pixel space to latent space, enhancing efficiency and scalability. Building on this foundation, DiT [31] and U-ViT [5] replace the traditional convolution-based U-Net [38] with Transformer architectures within the latent space, further improving performance. Flow matching [1, 25, 27] redefines the forward process as direct paths between the data distribution and a standard normal distribution, offering a more straightforward transition from noise to target data compared to conventional diffusion methods. SiT [2] leverages the backbone of DiT and employs flow matching to more directly connect these distributions. Scaling this concept, SD3 [15] introduces a novel Transformer-based architecture trained with flow matching for text-to-image generation. MAR [24] presents a diffusion-based strategy to model per-token probability distributions in a continuous space, enabling autoregressive

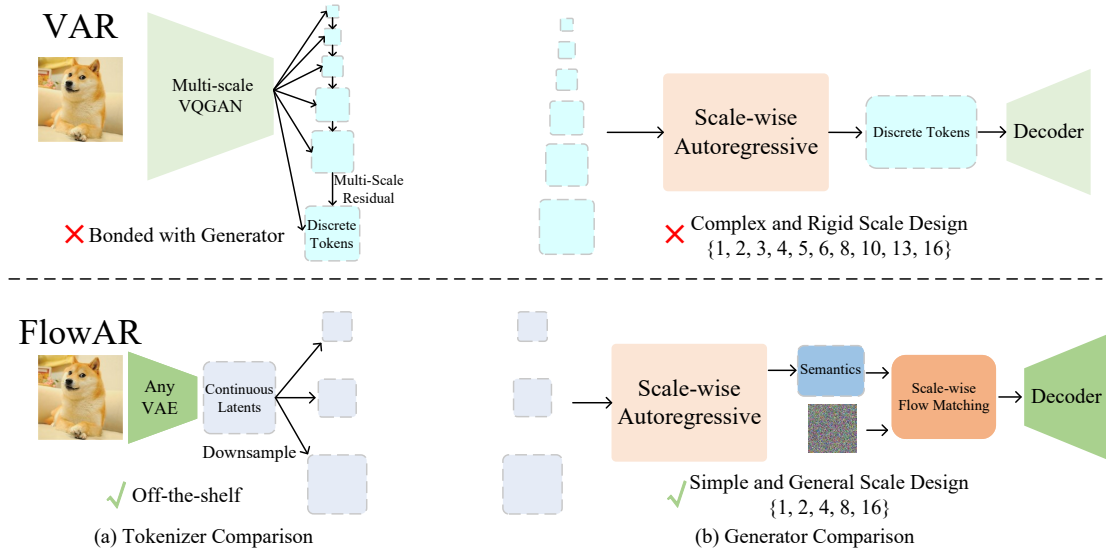


Figure 2. **Comparison Between VAR and Our FlowAR** in (a) Tokenizer and (b) Generator design. (a) VAR [44] utilizes a complex multi-scale residual VQGAN discrete tokenizer, whereas FlowAR can leverage any off-the-shelf VAE continuous tokenizer, constructing coarse scale token maps by directly downsampling the finest scale token map. (b) VAR’s generator is constrained by the same complex and rigid scale design as its tokenizer, while FlowAR benefits from a simple and flexible scale design, enhanced by the flow matching model.

models without relying on discrete tokenizers and utilizing a specialized diffusion loss function instead of the traditional categorical cross-entropy loss. In contrast to MAR, our proposed FlowAR employs a scale-wise flow matching model to capture per-scale probabilities, utilizing coarse-to-fine scale-wise conditioning derived from a scale-wise autoregressive model.

Discussion. Our FlowAR provides a more flexible framework for next scale prediction, enhanced with flow matching. In Figure 2, we compare our FlowAR model with VAR [44], highlighting key differences in both the tokenizer and generator components. For the tokenizer, VAR relies on a multi-scale VQGAN [14, 23, 36] that is tightly integrated with its generator and trained on a complex set of scales ($\{1, 2, 3, 4, 5, 6, 8, 10, 13, 16\}$). In contrast, FlowAR can use any off-the-shelf VAE [22] as its tokenizer, offering greater flexibility by constructing coarse scale token maps through direct downsampling of the finest scale token map. For the generator, VAR is constrained by a complex and rigid scale structure, whereas FlowAR benefits from a simpler and more general scale design, allowing the integration of the modern flow matching model [25].

3. Method

In this section, we begin with an overview of autoregressive modeling in Sec. 3.1, followed by a detailed introduction of the proposed method in Sec. 3.2.

3.1. Preliminary: Autoregressive Modeling

Autoregressive Modeling in NLP. Consider a corpus represented as a sequence of words $\mathcal{U} = \{w_1, w_2, \dots, w_n\}$. In NLP, autoregressive models predict each word based on all preceding words in the sequence:

$$p(\mathcal{U}) = \prod_{k=1}^n p(w_k | w_1, w_2, \dots, w_{k-1}, \Theta), \quad (1)$$

where the autoregressive model is parameterized by Θ . The objective function to minimize is the negative log-likelihood over the entire corpus:

$$\mathcal{L} = - \sum_{k=1}^n \log p(w_k | w_{<k}, \Theta), \quad (2)$$

where $<k$ denotes all positions preceding k . This approach serves as the foundation for successful large-scale language models, as demonstrated in [29, 30, 45].

Token-wise Autoregressive Modeling for Image Generation. Extending autoregressive modeling to images involves tokenizing a 2D image $X \in \mathbb{R}^{3 \times H \times W}$ using vector quantization [48]. This process converts the image into a grid of discrete tokens, which is subsequently flattened into a one-dimensional sequence $X = \{t_1, t_2, \dots, t_N\}$:

$$\mathcal{L} = - \sum_{k=1}^N \log p(t_k | t_{<k}, \Theta). \quad (3)$$

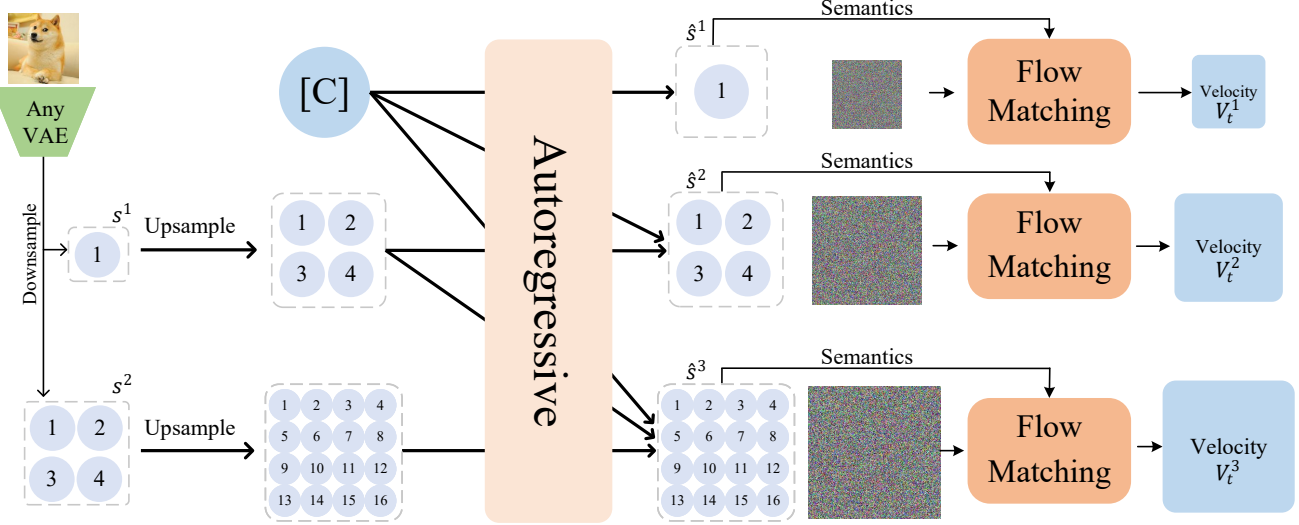


Figure 3. **Overview of The Proposed FlowAR.** FlowAR consists of three main components: (1) an off-the-shelf VAE that extracts a continuous latent representation of the image. We then create a set of coarse-to-fine scales by downsampling this latent, forming a sequence of token maps s^1, s^2, \dots, s^n , where each subsequent scale doubles in size from the previous one. (2) A scale-wise autoregressive Transformer that takes as input the sequence $\{[C], \text{Up}(s^1, 2), \dots, \text{Up}(s^{n-1}, 2)\}$, where $[C]$ is a condition token and $\text{Up}(\cdot, 2)$ denotes upsampling by a factor of 2. This Transformer generates semantic representations for different scales, $\hat{s}^1, \dots, \hat{s}^n$. (3) A scale-wise flow matching model, conditioned on the semantics \hat{s}^i at each scale i (time step conditions are not shown for simplicity), predicts the velocity given a random time step t that moves the noises to the target data distribution.

However, flattening the token grid disrupts the intrinsic two-dimensional spatial structure of the image. To preserve this spatial information, VAR [44] introduces a scale-wise autoregressive modeling approach, as described below.

Scale-wise Autoregressive Modeling for Image Generation. Rather than flattening images into token sequences, VAR [44] decomposes the image into a series of token maps across multiple scales, $S = \{s_1, s_2, \dots, s_n\}$. Each token map s_k has dimensions $h_k \times w_k$ and is obtained by a specially designed multi-scale VQGAN with residual structure [14, 23, 36, 44]. In contrast to single flattened tokens t_k that lose spatial context, each s_k maintains the two-dimensional structure with $h_k \times w_k$ tokens. The autoregressive loss function is then reformulated to predict each scale based on all preceding scales:

$$\mathcal{L} = -\sum_{k=1}^n \log p(s_k | s_{<k}, \Theta). \quad (4)$$

In this framework, generating the k -th scale in VAR requires attending to all previous scales $s_{<k}$ (*i.e.*, s_1 to s_{k-1}) and simultaneously predicting all $h_k \times w_k$ tokens in s_k via *categorical* distributions. The chosen scales, $S = \{1, 2, 3, 4, 5, 6, 8, 10, 13, 16\}$, introduce significant complexity to the scale design and constrain the model’s generalization capabilities. This is due to the tight coupling between the generator and tokenizer with the scale design, reducing flexibility in updating the tokenizer or support-

ing alternative scale configurations. Furthermore, VAR’s discrete tokenizer relies on a complex multi-scale residual structure, complicating the training process, with essential training code and details remaining publicly unavailable at the time of our submission.

3.2. Proposed Method: FlowAR

Overview. To address the issues outlined above, we introduce FlowAR seen in Figure 3, a more general scale-wise autoregressive modeling, enhanced with flow matching [25]. Our method incorporates two primary improvements over existing next scale prediction [44]: (1) replacing the multi-scale VQGAN discrete tokenizer with any off-the-shelf VAE continuous tokenizer [22], and (2) modeling the per-scale prediction (*i.e.*, predicting all $h_k \times w_k$ tokens in k -th scale s_k) using flow matching to learn the probability distribution. The first change enables the flexibility to leverage any existing VAE tokenizer, benefiting from recent advances in VAE technology without being constrained by a complex scale sequence design. The second improvement enhances generation quality by utilizing the modern flow matching algorithm.

Simple Scale Sequence with Any VAE Tokenizer. Given an image, we extract its *continuous* latent representation $F \in \mathbb{R}^{c \times h \times w}$ using an off-the-shelf Variational Autoencoder (VAE) [22]. We then construct a set of coarse-to-fine

scales by downsampling the latent F as follows:

$$\begin{aligned} S &= \{s^1, s^2, \dots, s^n\} \\ &= \{\text{Down}(F, 2^{n-1}), \text{Down}(F, 2^{n-2}), \dots, \text{Down}(F, 1)\}, \end{aligned} \quad (5)$$

where $\text{Down}(F, r)$ denotes downsampling the latent F by a factor of r , and no downsampling is applied when $r = 1$.

Notably, our multi-scale token maps S are derived by directly downsampling the highest-resolution latent F , removing the need for complex multi-scale residual VQGAN design [14, 23, 36, 44]. To distinguish our approach, we use the superscript i to denote our i -th scale token map, s^i . We set $n = 5$ (i.e., $S = \{1, 2, 4, 8, 16\}$), making the scale design in FlowAR significantly simpler and more versatile than that of VAR [44]. This design allows us to integrate various off-the-shelf VAE tokenizers into our framework, eliminating the need for a multi-scale tokenizer trained on a predefined scale sequence.

With this simplified scale sequence and the flexibility to use any off-the-shelf VAE tokenizer, we introduce our improvement for next scale prediction. Unlike VAR [44], which models the *categorical* distribution of each scale using an autoregressive Transformer, we utilize the Transformer to generate *conditioning* information for each scale, while a scale-wise flow matching model captures the scale’s probability distribution based on this information. Below, we outline how the autoregressive Transformer generates conditioning information for each scale, followed by details of the scale-wise flow matching module.

Generating Conditioning Information via Scale-wise Autoregressive Transformer. To produce the conditioning information for each subsequent scale, we utilize conditions obtained from all previous scales:

$$\hat{s}^i = T\left([C, \text{Up}(s^1, 2), \dots, \text{Up}(s^{i-1}, 2)]\right), \forall i = 1, \dots, n, \quad (6)$$

where $T(\cdot)$ represents the autoregressive Transformer model, C is the class condition, and $\text{Up}(s, r)$ denotes the upsampling of latent s by a factor of r . For the initial scale ($i = 1$), only the class condition C is used as input. We set $r = 2$, following our simple scale design, where each scale is double the size of the previous one. We refer to the resulting output \hat{s}^i as the *semantics* for the i -th scale, which is then used to condition a flow matching module to learn the per-scale probability distribution.

Scale-wise Flow Matching Model Conditioned by Autoregressive Transformer Output. Flow matching [25] generates samples from the target data distribution by gradually transforming a source noisy distribution, such as a Gaussian. For each i -th scale, FlowAR extends flow matching to generate the scale latent s^i , conditioned on the autoregressive Transformer’s output \hat{s}^i . Specifically, during

training, given the scale latent s^i from the target data distribution, we sample a time step $t \in [0, 1]$ and a source noise sample F_0^i from the source noisy distribution, typically setting $F_0^i \sim \mathcal{N}(0, 1)$ to match the shape of conditioned latent \hat{s}^i , analogous to the “noise” in diffusion models [37]. We then construct the interpolated input F_t^i as:

$$F_t^i = ts^i + (1 - t)F_0^i. \quad (7)$$

The model is trained to predict the velocity V_t^i using F_t^i :

$$\begin{aligned} V_t^i &= \frac{dF_t^i}{dt} \\ &= s^i - F_0^i, \end{aligned} \quad (8)$$

where V_t^i indicates the direction to move from F_t^i toward s^i , guiding the transformation from the source to the target distribution at each scale. Unlike prior approaches [2, 15] that condition velocity prediction on class or textual information, we condition on the scale-wise semantics \hat{s}^i from the autoregressive Transformer’s output. Notably, in prior methods [2, 15], the conditions and image latents often have different lengths, whereas FlowAR shares the same length (i.e., s^i and \hat{s}^i have the same shape, $\forall i = 1, \dots, n$). The training objective for scale-wise flow matching is:

$$\mathcal{L} = \sum_{i=1}^n \|\text{FM}(F_t^i, \hat{s}^i, t; \theta) - V_t^i\|^2, \quad (9)$$

where FM denotes the flow matching model parameterized by θ . This approach allows the model to capture scale-wise information bi-directionally, enhancing flexibility and efficiency in image generation within our framework.

Scale-wise Injection of Semantics via Spatial-adaLN. A key design choice is determining how best to inject the semantic information \hat{s}^i , generated by the autoregressive Transformer, into the flow matching module. A straightforward approach would be to concatenate the semantics \hat{s}^i with the flattened input F_t^i , similar to in-context conditioning [5] where the class condition is concatenated with the input sequence. However, this approach has two main drawbacks: (1) it increases the sequence length input to the flow matching model, raising computational costs, and (2) it provides indirect semantic injection, potentially weakening the effectiveness of semantic guidance. To address these issues, we propose using *spatially adaptive layernorm* for position-by-position semantic injection, resulting in the proposed Spatial-adaLN. Specifically, given the semantics \hat{s}^i from the scale-wise autoregressive Transformer and the intermediate feature $F_t^{i'}$ in the flow matching model, we inject the semantics to the scale γ , shift β , and gate α parameters of the adaptive normalization, following the standard adaptive normalization procedure [3, 31, 55]:

$$\begin{aligned}
\alpha_1, \alpha_2, \beta_1, \beta_2, \gamma_1, \gamma_2 &= \text{MLP}(\hat{s}^i + t), \\
\hat{F}_t^{i'} &= \text{Attn}(\gamma_1 \odot \text{LN}(F_t^{i'}) + \beta_1) \odot \alpha_1, \\
F_t^{i''} &= \text{MLP}(\gamma_2 \odot \text{LN}(\hat{F}_t^{i'}) + \beta_2) \odot \alpha_2,
\end{aligned}
\tag{10}$$

where Attn denotes the attention mechanism, and LN denotes the layer norm, $F_t^{i''}$ is the block’s output, and \odot is the spatial-wise product. Unlike traditional adaptive normalization, where the scale, shift, and gate parameters lack spatial information, our spatial adaptive normalization provides positional control, enabling dependency on semantics from the autoregressive Transformer. We apply the Spatial-adaLN to every Transformer block within the flow matching module. Alternative design choices are explored in the ablation study.

Inference Pipeline. At the beginning of inference, the autoregressive Transformer generates the initial semantics \hat{s}^1 using only the class condition C . This semantics \hat{s}^1 conditions the flow matching module, which gradually transforms a noise sample into the target distribution for s^1 . The resulting token map is upsampled by a factor of 2, combined with the class condition, and fed back into the autoregressive Transformer to generate the semantics \hat{s}^2 , which conditions the flow matching module for the next scale. This process is iterated n scales until the final token map s^n is estimated and subsequently decoded by the VAE decoder to produce the generated image. Notably, we use the KV cache [32] in the autoregressive Transformer to efficiently generate each semantics \hat{s}^i .

4. Experimental Results

In this section, we present our main results on the challenging ImageNet-256 generation benchmark [11] (Sec. 4.1), followed by ablation studies (Sec. 4.2).

4.1. Main Results

Following the settings in VAR [44], we train FlowAR on ImageNet-256 for class-conditional image generation. We evaluate the model using Fréchet Inception Distance (FID) [17] and inception score (IS) [39], Precision (Pre.) [33] and Recall (rec.) [33] as metrics.

Quantitative Results. As shown in Table 1, when compared to previous generative adversarial models [6, 20, 40], autoregressive models [14, 23, 36, 42, 51], diffusion-based methods [5, 12, 31, 37], and flow matching methods [2], FlowAR achieves significant performance gains. Specifically, our best model variant, FlowAR-H, attains an FID of 1.65, outperforming StyleGAN [40] (2.30), LlamaGen-3B [42] (2.18), DiT [31] (2.27), and SiT [2] (2.06).

Compared to the closely related VAR [44], FlowAR provides superior image quality at similar model scales. For example, FlowAR-L, with 589M parameters, achieves an FID of 1.90—surpassing both VAR-d20 (FID 2.95) of comparable size and even largest VAR-d30 (FID 1.97), which has 2B parameters. Furthermore, our largest model, FlowAR-H (1.9B parameters, FID 1.65), sets a new state-of-the-art benchmark for scale-wise autoregressive image generation.

Visualization. We visualize samples generated by FlowAR using different tokenizers in Figure 4, showing that FlowAR is capable of producing high-quality images with impressive visual fidelity and is compatible with various off-the-shelf VAEs. More samples are provided in the appendix.

4.2. Ablation Studies

Tokenizer Compatibility. VAR [44] relies on a complex multi-scale residual tokenizer that compresses images into discrete tokens at different scales, with the scale structure of the tokenizer directly mirroring VAR’s architectural scales. This tight coupling between the tokenizer and VAR limits the framework’s flexibility and adaptability. In contrast, our proposed FlowAR is compatible with a wide range of variational autoencoders (VAEs), enhancing versatility and ease of integration. As shown in Table 2, FlowAR achieves superior performance across various VAE architectures, including DC-AE [8] (FID of 4.22), SD-VAE [37] (FID of 3.94), and MAR-VAE [24] (FID of 3.61), compared to VAR’s multi-scale residual discrete tokenizer, which yields an FID of 5.81. These results underscore FlowAR’s effectiveness and adaptability, highlighting its advantage over VAR’s more rigid tokenizer dependency.

Construction of Scale Sequence. Instead of using a multi-scale VQGAN with residual connections, as in VAR [44], we propose a simpler approach by directly downsampling the latent representations extracted by any off-the-shelf continuous VAE [22] tokenizer. An alternative design choice would be to downsample the image before feeding it into a VAE. We explore this design choice in Table 3, where downsampling the latents (FID 3.61) significantly outperforms downsampling the image (FID 12.19).

Scale Configurations. To demonstrate FlowAR’s flexibility with respect to scale design, we perform an ablation study by progressively reducing the number of scales used in the model. Table 4 presents the results of this study. VAR [44] relies on a complex scale configuration with ten scales ($\{1, 2, 3, 4, 5, 6, 8, 10, 13, 16\}$) to achieve its reported performance. Simplifying VAR’s scale configuration to $\{1, 2, 4, 8, 16\}$ leads to training failure, indicating a strong dependency between its tokenizer and generator. In contrast, FlowAR demonstrates strong robustness to scale reduction. With the simplified sequence $\{1, 2, 4, 8, 16\}$, FlowAR achieves an FID of 3.61, outperforming VAR even with its full scale sequence. Reducing the scales further to

method	type	params	FID ↓	IS ↑	Pre. ↑	Rec. ↑
BigGAN [6]	GAN	112M	6.95	224.5	0.89	0.38
GigaGAN [20]	GAN	569M	3.45	225.5	0.84	0.61
StyleGAN [40]	GAN	166M	2.30	265.1	0.78	0.53
ADM [12]	diffusion	554M	10.94	101.0	0.69	0.63
LDM [37]	diffusion	400M	3.60	247.7	-	-
U-ViT[5]	diffusion	287M	3.40	219.9	0.83	0.52
DiT [31]	diffusion	675M	2.27	278.2	0.83	0.57
SiT [2]	flow matching	675M	2.06	270.3	0.82	0.59
VQVAE-2 [36]	token-wise autoregressive	13.5B	31.11	45.0	0.36	0.57
VQGAN [14]	token-wise autoregressive	1.4B	15.78	74.3	-	-
RQTransformer [23]	token-wise autoregressive	3.8B	7.55	134.0	-	-
LlamaGen-B [42]	token-wise autoregressive	111M	5.46	193.6	0.83	0.45
ViT-VQGAN [51]	token-wise autoregressive	1.7B	4.17	175.1	-	-
LlamaGen-L [42]	token-wise autoregressive	343M	3.07	256.1	0.83	0.52
LlamaGen-XL [42]	token-wise autoregressive	775M	2.62	244.1	0.80	0.57
LlamaGen-3B [42]	token-wise autoregressive	3.1B	2.18	263.3	0.81	0.58
VAR-d12 [44]	scale-wise autoregressive	132M	5.81	201.3	0.81	0.45
FlowAR-S	scale-wise autoregressive	170M	3.61	234.1	0.83	0.50
VAR-d16 [44]	scale-wise autoregressive	310M	3.55	280.4	0.84	0.51
FlowAR-B	scale-wise autoregressive	300M	2.90	272.5	0.84	0.54
VAR-d20 [44]	scale-wise autoregressive	600M	2.95	302.6	0.83	0.56
FlowAR-L	scale-wise autoregressive	589M	1.90	281.4	0.83	0.57
VAR-d30 [44]	scale-wise autoregressive	2.0B	1.97	323.1	0.82	0.59
FlowAR-H	scale-wise autoregressive	1.9B	1.65	296.5	0.83	0.60

Table 1. **Generation Results on ImageNet-256.** Metrics reported include Fréchet Inception Distance (FID), inception score (IS), precision (Pre.) and recall (Rec.). The proposed FlowAR demonstrates state-of-the-art generation performance. VAR is evaluated using code and pretrained weights from their official GitHub repository.

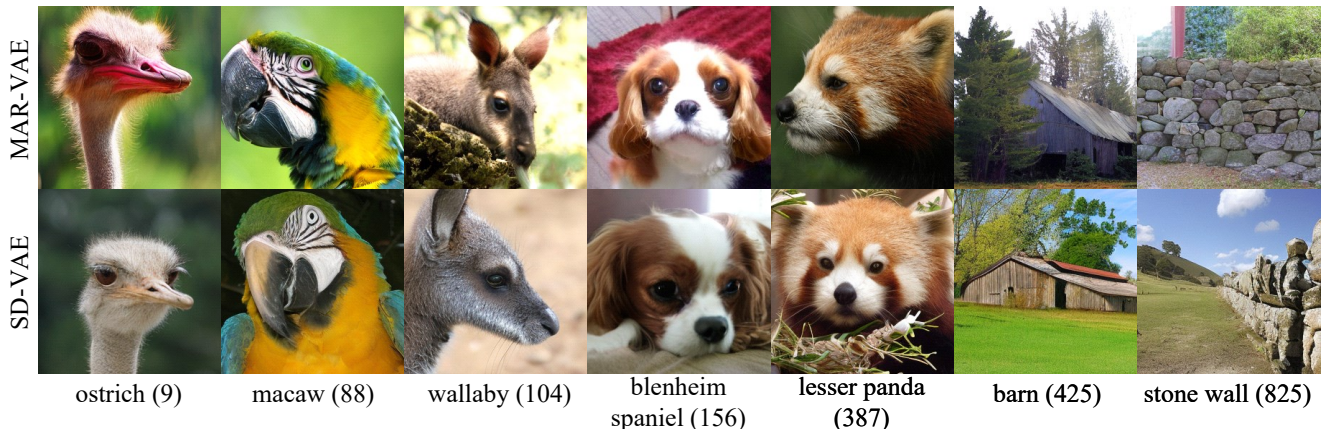


Figure 4. **Visualization of Samples Generated by FlowAR Using Different Tokenizers.** FlowAR consistently produces high-quality visual samples across various tokenizer configurations including VAE from MAR [24] and SD [37].

{1, 4, 8, 16}, FlowAR still maintains competitive performance with an FID of 4.88. Even with just three scales ({1, 4, 16}), FlowAR achieves an FID of 6.10, comparable to VAR’s FID of 5.81.

Scale-wise Flow Matching Model. The flow matching model is used to learn the *per-scale* probability distribu-

tion, predicting all $h_k \times w_k$ tokens in the k -th scale s_k . We consider two design alternatives. First, *per-scale* prediction could be replaced with *per-token* prediction using Multi-Layer Perceptrons (MLPs) [24], which, however, lacks the ability to capture interactions between tokens. Second, we could substitute the flow matching approach [25] with a dif-

tokenizer	generator	FID	IS
multi-scale residual VQGAN [44]	VAR [44]	5.81	201.3
DC-AE [8]	FlowAR	4.22	220.9
SD-VAE [37]	FlowAR	3.94	231.0
MAR-VAE [24]	FlowAR	3.61	234.1

Table 2. **Ablation on Tokenizer Compatibility.** While VAR [44] depends heavily on a multi-scale residual discrete tokenizer, FlowAR is compatible with a variety of continuous VAE tokenizers. The final setting is marked in gray.

scale construction	FID	IS
image	12.19	118.2
latent	3.61	234.1

Table 3. **Ablation on Construction of Scale Sequence.** We compare two approaches for constructing the scale sequence: down-sampling the input image before feeding it into the VAE, or down-sampling the latents extracted by the VAE. The final setting is highlighted in gray.

method	scales S	FID	IS
VAR [44]	{1, 2, 3, 4, 5, 6, 8, 10, 13, 16}	5.81	201.3
VAR [44]	{1, 2, 4, 8, 16}	N/A	N/A
FlowAR	{1, 2, 4, 8, 16}	3.61	234.1
FlowAR	{1, 4, 8, 16}	4.88	200.1
FlowAR	{1, 4, 16}	6.10	194.2

Table 4. **Ablation on Scale Configurations.** We compare VAR and FlowAR under various scale configurations. VAR is constrained by its predefined scale sequence and fails to generalize to other configurations (2nd row), whereas FlowAR demonstrates flexibility across different scale setups. The final setting is highlighted in gray.

per-token	per-scale	diffusion	flow-matching	FID	IS
✓		✓		6.85	155.6
✓			✓	6.15	184.1
	✓	✓		3.93	223.9
	✓		✓	3.61	234.1

Table 5. **Ablation on Scale-wise Flow Matching Model.** We investigate two design choices in this module: (1) per-token vs. per-scale prediction and (2) diffusion vs. flow-matching framework. The final setting is highlighted in gray.

fusion framework [18]. These design choices are explored in Table 5, where *per-scale* prediction consistently outperforms *per-token* prediction, regardless of whether flow matching or diffusion is used. Additionally, flow matching provides marginal improvements over the diffusion framework. Our final model configuration employs *per-scale* prediction with the flow matching framework.

Injection of Semantics. There are several methods to inject the semantics \hat{s}^i , generated by the autoregressive Transformer, into the flow matching module. We summarize

injection of semantics	FID	IS
adaLN	14.28	111.9
sequence concatenation	9.22	146.9
addition	6.22	188.2
cross attention	5.37	202.5
channel concatenation	4.85	210.9
spatial-adaLN	3.61	234.1

Table 6. **Ablation on Semantic Injection Schemes for the Flow Matching Module.** The proposed Spatial-adaLN injects semantics in a spatially adaptive manner, achieving the best performance. The final setting is highlighted in gray.

these methods in Table 6: (1) ‘addition’: Element-wise addition of the semantics and the flattened input. (2) ‘cross attention’: Using cross-attention where the flattened input serves as the query and the semantics act as the key and value. (3) ‘sequence concatenation’: Concatenating the semantics with the flattened input along the sequence dimension. (4) ‘channel concatenation’: Concatenating the semantics with the flattened input along the channel dimension. (5) ‘adaLN’: Adaptive LayerNorm conditioned on the spatially averaged semantics. (6) ‘Spatial-adaLN’: The proposed spatial adaptive LayerNorm, injecting semantics position-by-position.

As shown in Table 6, the choice of semantic injection method significantly impacts performance. The proposed ‘Spatial-adaLN’ achieves the best results, with an FID of 3.61 and an Inception Score (IS) of 234.1, outperforming all other methods. These results indicate that methods preserving spatial structures and offering position-wise semantic guidance yield superior image generation quality. The exceptional performance of Spatial-adaLN can be attributed to its ability to inject semantics directly into the normalization layers in a spatially adaptive manner, effectively capturing fine-grained details and enhancing the model’s capacity to generate high-fidelity images.

5. Conclusion

In this work, we presented FlowAR, a flexible and generalized approach to scale-wise autoregressive modeling for image generation, enhanced with flow matching for improved quality. By adopting a streamlined scale design and compatible with any VAE tokenizer, FlowAR addresses limitations of prior models, offering greater adaptability and superior image quality. With spatially adaptive layer normalization, it effectively captures fine-grained details, achieving state-of-the-art results on ImageNet-256 generation benchmark. We hope FlowAR will inspire more future research in autoregressive image modeling.

References

- [1] Michael S Albergo and Eric Vanden-Eijnden. Building normalizing flows with stochastic interpolants. *arXiv preprint arXiv:2209.15571*, 2022. 2
- [2] Sara Atito, Muhammad Awais, and Josef Kittler. Sit: Self-supervised vision transformer. *arXiv preprint arXiv:2104.03602*, 2021. 2, 5, 6, 7
- [3] Jimmy Lei Ba, Jamie Ryan Kiros, and Geoffrey E Hinton. Layer normalization. *arXiv preprint arXiv:1607.06450*, 2016. 2, 5
- [4] Jinze Bai, Shuai Bai, Yunfei Chu, Zeyu Cui, Kai Dang, Xiaodong Deng, Yang Fan, Wenbin Ge, Yu Han, Fei Huang, et al. Qwen technical report. *arXiv preprint arXiv:2309.16609*, 2023. 2
- [5] Fan Bao, Shen Nie, Kaiwen Xue, Yue Cao, Chongxuan Li, Hang Su, and Jun Zhu. All are worth words: A vit backbone for diffusion models. In *CVPR*, 2023. 2, 5, 6, 7
- [6] Andrew Brock, Jeff Donahue, and Karen Simonyan. Large scale gan training for high fidelity natural image synthesis. arxiv 2018. *arXiv preprint arXiv:1809.11096*, 1809. 6, 7
- [7] Tom B. Brown, Benjamin Mann, Nick Ryder, Melanie Subbiah, Jared Kaplan, Prafulla Dhariwal, Arvind Neelakantan, Pranav Shyam, Girish Sastry, Amanda Askell, et al. Language models are few-shot learners. *NeurIPS*, 2020. 1, 2
- [8] Junyu Chen, Han Cai, Junsong Chen, Enze Xie, Shang Yang, Haotian Tang, Muyang Li, Yao Lu, and Song Han. Deep compression autoencoder for efficient high-resolution diffusion models. *arXiv preprint arXiv:2410.10733*, 2024. 2, 6, 8
- [9] Mark Chen, Alec Radford, Rewon Child, Jeff Wu, Heewoo Jun, Prafulla Dhariwal, David Luan, and Ilya Sutskever. Generative pretraining from pixels. In *ICML*, 2020. 2
- [10] Aakanksha Chowdhery, Sharan Narang, Jacob Devlin, Maarten Bosma, Gaurav Mishra, Adam Roberts, Paul Barham, Hyung Won Chung, Charles Sutton, Sebastian Gehrmann, et al. Palm: Scaling language modeling with pathways. *Journal of Machine Learning Research*, 24(240): 1–113, 2023. 2
- [11] Jia Deng, Wei Dong, Richard Socher, Li-Jia Li, Kai Li, and Li Fei-Fei. Imagenet: A large-scale hierarchical image database. In *CVPR*, 2009. 2, 6
- [12] Prafulla Dhariwal and Alexander Nichol. Diffusion models beat gans on image synthesis. *NeurIPS*, 34, 2021. 6, 7
- [13] Abhimanyu Dubey, Abhinav Jauhri, Abhinav Pandey, Abhishek Kadian, Ahmad Al-Dahle, Aiesha Letman, Akhil Mathur, Alan Schelten, Amy Yang, Angela Fan, et al. The llama 3 herd of models. *arXiv preprint arXiv:2407.21783*, 2024. 2
- [14] Patrick Esser, Robin Rombach, and Bjorn Ommer. Taming transformers for high-resolution image synthesis. In *CVPR*, 2021. 1, 2, 3, 4, 5, 6, 7
- [15] Patrick Esser, Sumith Kulal, Andreas Blattmann, Rahim Entezari, Jonas Müller, Harry Saini, Yam Levi, Dominik Lorenz, Axel Sauer, Frederic Boesel, et al. Scaling rectified flow transformers for high-resolution image synthesis. In *ICML*, 2024. 2, 5
- [16] Ian Goodfellow, Jean Pouget-Abadie, Mehdi Mirza, Bing Xu, David Warde-Farley, Sherjil Ozair, Aaron Courville, and Yoshua Bengio. Generative adversarial nets. *NeurIPS*, 2014. 2
- [17] Martin Heusel, Hubert Ramsauer, Thomas Unterthiner, Bernhard Nessler, and Sepp Hochreiter. Gans trained by a two time-scale update rule converge to a local nash equilibrium. *NeurIPS*, 30, 2017. 6
- [18] Jonathan Ho, Ajay Jain, and Pieter Abbeel. Denoising diffusion probabilistic models. *NeurIPS*, 2020. 2, 8
- [19] Emiel Hoogeboom, Jonathan Heek, and Tim Salimans. simple diffusion: End-to-end diffusion for high resolution images. In *ICML*, 2023. 2
- [20] Minguk Kang, Jun-Yan Zhu, Richard Zhang, Jaesik Park, Eli Shechtman, Sylvain Paris, and Taesung Park. Scaling up gans for text-to-image synthesis. In *CVPR*, 2023. 6, 7
- [21] Diederik P Kingma and Jimmy Ba. Adam: A method for stochastic optimization. In *ICLR*, 2015. 11
- [22] Diederik P Kingma and Max Welling. Auto-encoding variational bayes. In *ICLR*, 2014. 2, 3, 4, 6
- [23] Doyup Lee, Chiheon Kim, Saehoon Kim, Minsu Cho, and Wook-Shin Han. Autoregressive image generation using residual quantization. In *CVPR*, 2022. 2, 3, 4, 5, 6, 7
- [24] Tianhong Li, Yonglong Tian, He Li, Mingyang Deng, and Kaiming He. Autoregressive image generation without vector quantization. *NeurIPS*, 2024. 2, 6, 7, 8
- [25] Yaron Lipman, Ricky TQ Chen, Heli Ben-Hamu, Maximilian Nickel, and Matt Le. Flow matching for generative modeling. *arXiv preprint arXiv:2210.02747*, 2022. 2, 3, 4, 5, 7
- [26] Qihao Liu, Zhanpeng Zeng, Ju He, Qihang Yu, Xiaohui Shen, and Liang-Chieh Chen. Alleviating distortion in image generation via multi-resolution diffusion models. *NeurIPS*, 2024. 2
- [27] Xingchao Liu, Chengyue Gong, and Qiang Liu. Flow straight and fast: Learning to generate and transfer data with rectified flow. *arXiv preprint arXiv:2209.03003*, 2022. 2
- [28] Ilya Loshchilov and Frank Hutter. Decoupled weight decay regularization. In *ICLR*, 2019. 11
- [29] OpenAI. Introducing chatgpt. <https://openai.com/blog/chatgpt/>, 2022. 1, 3
- [30] OpenAI. Gpt-4 technical report. *arXiv preprint arXiv:2303.08774*, 2023. 1, 2, 3
- [31] William Peebles and Saining Xie. Scalable diffusion models with transformers. In *ICCV*, 2023. 2, 5, 6, 7
- [32] Reiner Pope, Sholto Douglas, Aakanksha Chowdhery, Jacob Devlin, James Bradbury, Jonathan Heek, Kefan Xiao, Shivani Agrawal, and Jeff Dean. Efficiently scaling transformer inference. *Proceedings of Machine Learning and Systems*, 5, 2023. 6
- [33] David MW Powers. Evaluation: from precision, recall and f-measure to roc, informedness, markedness and correlation. *arXiv preprint arXiv:2010.16061*, 2020. 6
- [34] Alec Radford, Karthik Narasimhan, Tim Salimans, and Ilya Sutskever. Improving language understanding by generative pre-training. https://cdn.openai.com/research-covers/language-unsupervised/language_understanding_paper.pdf, 2018. 2

- [35] Alec Radford, Jong Wook Kim, Chris Hallacy, Aditya Ramesh, Gabriel Goh, Sandhini Agarwal, Girish Sastry, Amanda Askell, Pamela Mishkin, Jack Clark, Gretchen Krueger, and Ilya Sutskever. Learning transferable visual models from natural language supervision. In *ICML*, 2021. 2
- [36] Ali Razavi, Aaron Van den Oord, and Oriol Vinyals. Generating diverse high-fidelity images with vq-vae-2. *NeurIPS*, 2019. 2, 3, 4, 5, 6, 7
- [37] Robin Rombach, Andreas Blattmann, Dominik Lorenz, Patrick Esser, and Björn Ommer. High-resolution image synthesis with latent diffusion models. In *CVPR*, 2022. 2, 5, 6, 7, 8
- [38] Olaf Ronneberger, Philipp Fischer, and Thomas Brox. U-net: Convolutional networks for biomedical image segmentation. In *MICCAI*, 2015. 2
- [39] Tim Salimans, Ian Goodfellow, Wojciech Zaremba, Vicki Cheung, Alec Radford, and Xi Chen. Improved techniques for training gans. *NeurIPS*, 29, 2016. 6
- [40] Axel Sauer, Katja Schwarz, and Andreas Geiger. Stylegan-xl: Scaling stylegan to large diverse datasets. *arXiv preprint arXiv:2201.00273*, 2022. 2, 6, 7
- [41] Jiaming Song, Chenlin Meng, and Stefano Ermon. Denoising diffusion implicit models. *arXiv preprint arXiv:2010.02502*, 2020. 2
- [42] Peize Sun, Yi Jiang, Shoufa Chen, Shilong Zhang, Bingyue Peng, Ping Luo, and Zehuan Yuan. Autoregressive model beats diffusion: Llama for scalable image generation. *arXiv preprint arXiv:2406.06525*, 2024. 1, 2, 6, 7
- [43] Gemini Team, Rohan Anil, Sebastian Borgeaud, Yonghui Wu, Jean-Baptiste Alayrac, Jiahui Yu, Radu Soricut, Johan Schalkwyk, Andrew M Dai, Anja Hauth, et al. Gemini: a family of highly capable multimodal models. *arXiv preprint arXiv:2312.11805*, 2023. 2
- [44] Keyu Tian, Yi Jiang, Zehuan Yuan, Bingyue Peng, and Liwei Wang. Visual autoregressive modeling: Scalable image generation via next-scale prediction. *NeurIPS*, 2024. 1, 2, 3, 4, 5, 6, 7, 8, 11
- [45] Hugo Touvron, Thibaut Lavril, Gautier Izacard, Xavier Martinet, Marie-Anne Lachaux, Timothée Lacroix, Baptiste Rozière, Naman Goyal, Eric Hambro, Faisal Azhar, et al. Llama: Open and efficient foundation language models. *arXiv preprint arXiv:2302.13971*, 2023. 2, 3
- [46] Hugo Touvron, Louis Martin, Kevin Stone, Peter Albert, Amjad Almahairi, Yasmine Babaei, Nikolay Bashlykov, Soumya Batra, Prajjwal Bhargava, Shruti Bhosale, et al. Llama 2: Open foundation and fine-tuned chat models. *arXiv preprint arXiv:2307.09288*, 2023. 2
- [47] Aaron Van den Oord, Nal Kalchbrenner, Lasse Espeholt, Oriol Vinyals, Alex Graves, et al. Conditional image generation with pixelcnn decoders. *NeurIPS*, 2016. 2
- [48] Aaron Van Den Oord, Oriol Vinyals, et al. Neural discrete representation learning. *NeurIPS*, 2017. 2, 3
- [49] A Vaswani. Attention is all you need. *NeurIPS*, 2017. 2, 11
- [50] Mark Weber, Lijun Yu, Qihang Yu, Xueqing Deng, Xiaohui Shen, Daniel Cremers, and Liang-Chieh Chen. Maskbit: Embedding-free image generation via bit tokens. *arXiv preprint arXiv:2409.16211*, 2024. 2
- [51] Jiahui Yu, Xin Li, Jing Yu Koh, Han Zhang, Ruoming Pang, James Qin, Alexander Ku, Yuanzhong Xu, Jason Baldridge, and Yonghui Wu. Vector-quantized image modeling with improved vqgan. *arXiv preprint arXiv:2110.04627*, 2021. 6, 7
- [52] Jiahui Yu, Yuanzhong Xu, Jing Yu Koh, Thang Luong, Gunjan Baid, Zirui Wang, Vijay Vasudevan, Alexander Ku, Yinfei Yang, Burcu Karagol Ayan, et al. Scaling autoregressive models for content-rich text-to-image generation. *arXiv preprint arXiv:2206.10789*, 2022. 1, 2
- [53] Qihang Yu, Ju He, Xueqing Deng, Xiaohui Shen, and Liang-Chieh Chen. Randomized autoregressive visual generation. *arXiv preprint arXiv:2411.00776*, 2024. 2
- [54] Qihang Yu, Mark Weber, Xueqing Deng, Xiaohui Shen, Daniel Cremers, and Liang-Chieh Chen. An image is worth 32 tokens for reconstruction and generation. *NeurIPS*, 2024. 2
- [55] Biao Zhang and Rico Sennrich. Root mean square layer normalization. *NeurIPS*, 2019. 5

Appendix

The appendix includes the following additional information:

- Sec. A lists the hyper-parameters of FlowAR.
- Sec. B provides the architectural details of FlowAR model variants.
- Sec. C provides more visualization results.

A. Hyper-parameters

We list the hyper-parameters of our FlowAR in Table 7.

training hyper-parameters	
optimizer	AdamW [21, 28]
warmup epochs	100
total epochs	400
batch size	1024
peak learning rate	2e-4
minimal learning rate	1e-5
learning rate schedule	cosine
class label dropout rate	0.1
max gradient norm	1.0

Table 7. Hyper-parameters of FlowAR.

B. Model Variants

In Table 8, we provide four kinds of different configurations of FlowAR for a fair comparison under similar parameters with VAR [44]. The proposed FlowAR contains two main modules: Autoregressive Model and Flow Matching Model, both build on top of Transformer architectures [49].

variants	autoregressive model	flow matching model
FlowAR-S	D=12, W=768	D=2, W= 1024
FlowAR-B	D=16, W= 768	D=6, W=1024
FlowAR-L	D=16, W= 1024	D=12, W= 1024
FlowAR-H	D=30, W= 1536	D=18, W= 1536

Table 8. **Model Variants.** “D” and “W” represent model depth and width, respectively.

C. More Visualization Results

Additional visualization results generated by FlowAR-H are provided from Figure 5 to Figure 12.



Figure 5. **Generated samples from FlowAR.** FlowAR generate high-fidelity great grey owl (24) images.



Figure 6. **Generated samples from FlowAR.** FlowAR generate high-fidelity macaw (88) images.



Figure 7. **Generated samples from FlowAR.** FlowAR generate high-fidelity golden retriever (207) images.



Figure 9. **Generated samples from FlowAR.** FlowAR generate high-fidelity lesser panda (387) images.



Figure 8. **Generated samples from FlowAR.** FlowAR generate high-fidelity otter (360) images.



Figure 10. **Generated samples from FlowAR.** FlowAR generate high-fidelity artichoke (944) images.



Figure 11. **Generated samples from FlowAR.** FlowAR generate high-fidelity alp (970) images.



Figure 12. **Generated samples from FlowAR.** FlowAR generate high-fidelity valley (979) images.